9-1999

Neutron Resonance Spectroscopy of 103Rh from 30 eV to 2 keV

D A. Smith
Los Alamos National Laboratory

J D. Bowman
Los Alamos National Laboratory

Bret E. Crawford
Gettysburg College

See next page for additional authors

Smith, D. A., Bowman, J. D., Crawford, B. E., Grossmann, C. A., Haseyama, T., Masaike, A., Matsuda, Y., Mitchell, G. E., Penttila, S. I., Roberson, N. R., Seestrom, S. J., Sharapov, E. I., Stephenson, S., & Yuan, V. W. (1999). Neutron Resonance Spectroscopy of 103Rh from 30 eV to 2 keV. Physical Review C, 60(045502). http://dx.doi.org/10.1103/PhysRevC.60.045502

Neutron Resonance Spectroscopy of 103Rh from 30 eV to 2 keV

Abstract

Neutron resonances in ^{103}Rh have been measured for neutron energies from 30 to 2000 eV using the time-of-flight method and the (n,γ) reaction. The rhodium resonance spectroscopy is essential for the analysis of parity violation measurements recently performed on neutron resonances in ^{103}Rh. Neutron scattering and radiative widths were determined, and orbital angular momentum assignments made with a Bayesian analysis. The s-wave and p-wave strength functions and average level spacings were determined.

Disciplines

Atomic, Molecular and Optical Physics | Physics

Authors

D A. Smith, J D. Bowman, Bret E. Crawford, C A. Grossmann, T Haseyama, A Masaike, Y Matsuda, G E. Mitchell, S I. Penttila, N R. Roberson, S J. Seestrom, E I. Sharapov, Sharon L. Stephenson, and V W. Yuan

Neutron resonance spectroscopy of ^{103}Rh from 30 eV to 2 keV

D. A. Smith,[1] J. D. Bowman,[1] B. E. Crawford,[2,*] C. A. Grossmann,[3] T. Haseyama,[4] A. Masaike,[4,†] Y. Matsuda,[4,‡] G. E. Mitchell,[3] S. I. Penttila,[1] N. R. Roberson,[2] S. J. Seestrom,[1] E. I. Sharapov,[5] S. L. Stephenson,[3,*] and V. Yuan[1]

[1]*Los Alamos National Laboratory, Los Alamos, New Mexico 87545*

[2]*Duke University, Durham, North Carolina 27708 and Triangle Universities Nuclear Laboratory, Durham, North Carolina 27708-0308*

[3]*North Carolina State University, Raleigh, North Carolina 27695-8202 and Triangle Universities Nuclear Laboratory, Durham, North Carolina 27708-0308*

[4]*Physics Department, Kyoto University, Kyoto 606-01, Japan*

[5]*Joint Institute for Nuclear Research, RU-141980 Dubna, Russia*

(Received 7 April 1999; published 16 September 1999)

Neutron resonances in ^{103}Rh have been measured for neutron energies from 30 to 2000 eV using the time-of-flight method and the (n,γ) reaction. The rhodium resonance spectroscopy is essential for the analysis of parity violation measurements recently performed on neutron resonances in ^{103}Rh. Neutron scattering and radiative widths were determined, and orbital angular momentum assignments made with a Bayesian analysis. The s-wave and p-wave strength functions and average level spacings were determined.
[S0556-2813(99)06410-9]

PACS number(s): 25.40.Ny, 11.30.Er, 27.90.+b

I. INTRODUCTION

Following the observation of an extremely large enhancement of parity violation for neutron resonances in heavy nuclei [1], a new approach to symmetry breaking has been developed. The symmetry-breaking matrix elements are treated as random variables, and the experimental goal is the measurement of the root-mean-square symmetry-breaking matrix element. This new approach to parity nonconservation (PNC) is discussed in recent reviews [2–4]. The TRIPLE Collaboration was formed to study parity violation in neutron resonances utilizing the high neutron flux available at the Manuel Lujan Neutron Scattering Center at the Los Alamos Neutron Science Center (LANSCE). Our initial focus was on ^{238}U and ^{232}Th. We observed many parity violations in ^{238}U and ^{232}Th and determined a rms PNC matrix element [5–8]. These measurements were in the vicinity of the $4p$ neutron strength function maximum. To determine the mass dependence of the effective nucleon-nucleus weak interaction, it is necessary to perform the PNC measurements in other mass regions. Since these experiments require that the p-wave resonances be observable, the most favorable other mass region is near the $3p$ neutron strength function maximum in the vicinity of $A=100$.

The magnitude of the observed PNC effects is proportional to the level density, and the average level density increases with mass number A. One can compensate for the lower average level density at lower masses by studying odd-mass targets in the $A=100$ region. For targets with spin the spectroscopy is much more complicated—two s-wave resonance spins, four p-wave resonance spins, and entrance channel mixing [9]. In order to extract the rms PNC matrix element from the data, the resonance parameters for both the s-wave and p-wave neutron resonances are needed. Although one can average over unknown parameters, this averaging increases the uncertainty in the determination of the PNC matrix elements [9]. Thus a prerequisite for PNC analysis is knowledge of the relevant neutron resonance spectroscopy.

The nuclide ^{103}Rh seemed an excellent candidate for PNC measurement, since it is monoisotopic, has a favorable level density (total observed level spacing about 16 eV), and is near the $3p$ strength function maximum. A number of parity violations have been observed in ^{103}Rh [10] by our group. With the high neutron flux available at the Manuel Lujan Neutron Scattering Center, we also were able to improve the neutron resonance spectroscopy of ^{103}Rh.

II. EXPERIMENTAL PROCEDURE

The data were measured at flight path 2 of the Manuel Lujan Neutron Scattering Center. The 800-MeV H^- beam from the LANSCE linac is deflected and transported to the Proton Storage Ring (PSR). The negative beam is neutralized, injected into the PSR, and converted to protons by stripping in a thin foil. The injected beam is stacked onto itself until protons from the entire linac macropulse are stored. The net result is that the proton pulse is reduced from about 800 μs to about 250 ns. The extracted proton beam strikes a tungsten target, and neutrons are created by the spallation process. These neutrons are moderated using a chilled water moderator [11] and then collimated. The neutron energy was determined from the time-of-flight over a 59.4-m distance from source to detector.

The detector is an array of 24 CsI(pure) crystals placed around the interaction target, providing approximately 3.0π of detection solid angle. The crystals are packed tightly around the target in two arrays of 12 crystals each, with a 20-cm cylindrical hole through the middle to allow access

*Present address: Gettysburg College, Gettysburg, PA 17325.

†Present address: Fukui University of Technology, 3-6-1 Gakuen Fukui-shi, 910-8505, Japan.

‡Present address: Institute of Physical and Chemical Research (RIKEN), Saitama 351-0198, Japan.

for the ^{6}Li-loaded polyethylene insert and for the neutron beam [12–14]. The crystals are 15-cm long wedges that form annular rings of 20-cm inner diameter and 40-cm outer diameter. The scintillation light from the CsI crystals is detected by photomultiplier tubes (PMT). The PMT signals are converted to logic pulses by constant fraction discriminators, and these pulses are counted by a multiscaler attached to an averaging memory. The start time of the multiscaler spectrum is derived from the proton pulse. In order to reduce the background a coincidence of two detector signals was required for an event to be recorded. The multiscaler dwell time (channel width) was set to 100 ns with a spectrum length of 8192 time-of-flight channels. This gives a time-of-flight range of 0 to 0.8192 ms, which corresponds to neutron energies from 30 eV to 2 keV. More detailed description of the detector shielding and electronics is provided by Seestrom *et al.* [14].

The target was assembled from plates of natural rhodium metal (100% ^{103}Rh, 99.9% chemically pure) in the form of a 10-cm diameter disk of areal density 2.99 g/cm^2. This target was placed directly between the two arrays of CsI crystals. By comparison with known resonances, a number of impurities were identified—ruthenium, palladium, silver, iridium, platinum, and gold. By fitting to strong s-wave resonances in these nuclei, the amount of each contaminant nuclide was determined. Using known resonance parameters the effects of these contaminant resonances were included in our analysis. A typical spectrum measured in this experiment is shown in Fig. 1. The number of counts in each 0.1 μs time-of-flight bin is plotted versus neutron energy.

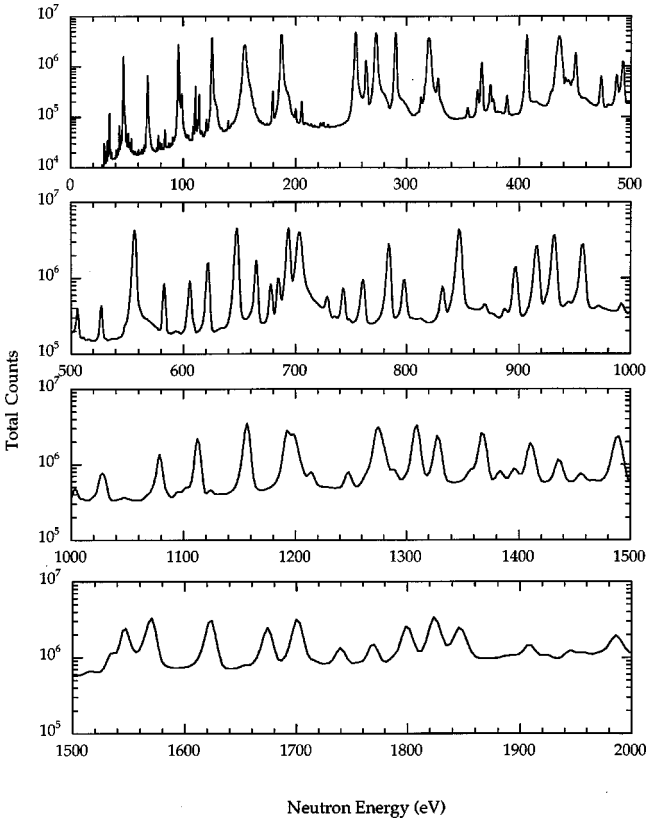

FIG. 1. Neutron time-of-flight spectrum for ^{103}Rh. The spectrum from 1 to 30 eV has been relatively normalized to the data from 30 to 2000 eV and plotted on the same scale.

III. RESONANCE STRENGTHS

The time-of-flight spectra were analyzed using the fitting code FITXS [15]. This program was developed by the TRIPLE Collaboration for the analysis of neutron resonances, where the neutrons are created with a moderated pulsed neutron beam. The analysis program can be used to determine resonance parameters for data measured by neutron transmission or by radiative capture. The code includes all major resolution effects that are observed in the neutron time-of-flight spectra. Effects of moderation time, detector efficiencies, beam length, target temperature, pulse width, etc., can be included, and the resonance parameters (E_0, $g\Gamma_n$, and total Γ_γ) can be determined by fitting directly to the data. Details of the application of this analysis program are described by Crawford *et al.* [7].

A sample fit for a time-of-flight region near 100 eV is shown in Fig. 2. In the figure neutron counts per 0.1 μs time-of-flight bin are plotted versus time-of-flight, with the fit to the data shown as a solid curve. Most of the major analysis difficulties are illustrated by this figure. There are five p-wave resonances and one s-wave resonance in ^{103}Rh in this energy range, and there are also resonances from iridium, palladium, and platinum, along with the background. The contaminant resonances and the rhodium s-wave resonance must be fit along with the rhodium p-wave resonances in order to determine the resonance parameters accurately. In this section of the spectrum the multiple-scattering peak for the one s-wave resonance at 95 eV is visible as a broad shoulder on the high energy side of the resonance. Multiple-scattering effects are discussed below. As is clear from the figure, the resonances were all well fit with the FITXS code.

The data were corrected for the detector dead time, or count rate efficiency. The neutron flux for the experiment was as high as the γ-ray detector allowed, since very good statistics were needed for the parity violation measurements. The normal high count rate runs were compared to a run that was taken with one tenth of the high count rate in order to determine the count rate efficiency. Both the efficiency due to count rate, and the differences in background were then corrected in the high count rate runs. The other calibrations could then be performed by starting with the known resonance parameters for ^{103}Rh [16,17].

A time offset (from the beginning of the multiscaler data) was observed in the spectra. This offset was a constant for all data measured during that beam cycle and has the value 1.55 ± 0.05 μs, where the error in the offset is one half the multiscaler dwell time. The beam length for the time-of-flight measurements was determined by fitting peaks to the energies of known neutron resonances. This calibration was performed using resonances from all targets placed in the beam during that run cycle—^{103}Rh, ^{117}Sn, ^{127}I, and ^{232}Th. In practice the ^{232}Th resonances provided the greatest accuracy for the neutron resonance energies and the best determination of the flight path length, which was 59.390 ± 0.014 m. The errors in determining the flight path length

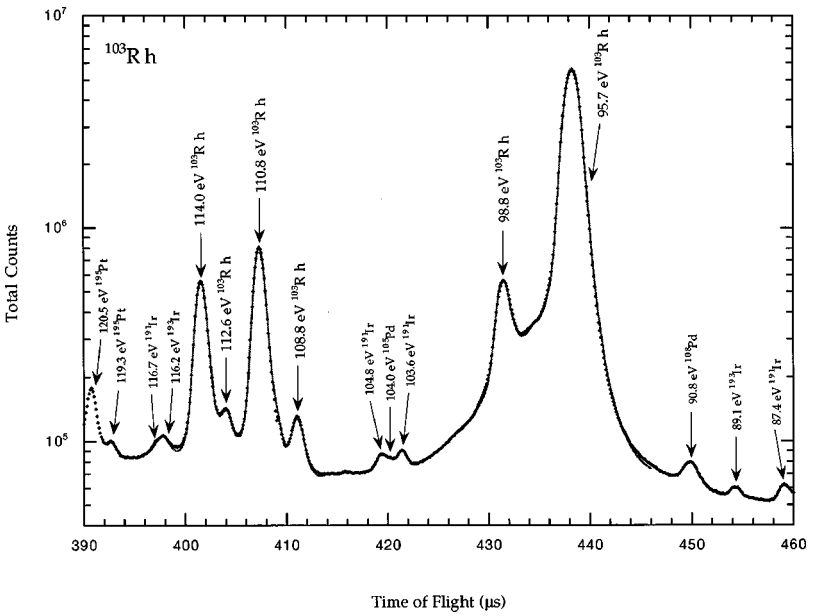

FIG. 2. Fit to a section of the time-of-flight spectrum. The data are plotted as points and the fit obtained with the code FITXS is shown as a line.

and the time offset are the dominant systematic errors in the measured energies of the neutron resonances, since the statistical errors on the energy measurement are on the order of 0.001%.

A problem in the data analysis was the presence of neutron capture after multiple scattering in the sample. In our rhodium target, approximately 10% of incoming neutrons were scattered in the first interaction due to s-wave potential elastic scattering. Detailed numerical estimates of the multiple-scattering contribution have been performed with a Monte Carlo code [18] for a parallel experiment on ^{117}Sn performed under the same experimental conditions. Since the rhodium target is a factor of two thinner than the tin target, the multiscattering corrections should be smaller. The neutron energy loss averaged over all scattering angles is $\Delta E \simeq 2E/A$, and neutrons with an energy $E=E_0+\Delta E$ higher than the resonance energy E_0 are effectively captured after scattering. Multiple scattering produces an additional peak or shoulder at the higher energy side of a resonance in the time-of-flight spectrum depending on whether the ΔE value is larger or smaller than the resonance width (in our case, the observed experimental width is determined by the Doppler width below $E \simeq 200$ eV and the instrumental width above 200 eV). For most of the resonances below 1 keV, the secondary peaks could be approximated as artificial peaks, which minimized their influence in fitting the actual resonances.

The neutron flux and detector efficiencies were calibrated by fitting to known resonance parameters for s-wave and p-wave resonances in ^{103}Rh after subtracting the multiple scattering peaks. There might be different detector efficiencies for s-wave and p-wave resonances, due to the differing multiplicities of the capture γ-rays produced. However, our analysis gave the same efficiency for the two types of resonances. Before the neutron flux could be determined by fitting to resonance parameters, effects due to material in the beam line had to be included. The beam passed through thin aluminum windows that did not affect the neutron beam appreciably. However, trace amounts of manganese did reduce the neutron flux in the vicinity of the large neutron resonance in manganese near 340 eV.

The energy dependence of the neutron flux is known to be a power law in the neutron energy, $\Phi(E)=cE^{-p}$ [19]. Fitting the data to known neutron resonance parameters led to a 5% uncertainty in both c and p. The uncertainty in the exponent is governed by the accuracy of the resonance parameters for ^{103}Rh. Other data measured that year included neutron flux measurements with ^{3}He scintillation detectors [20]. The energy dependence of these detectors was determined very accurately, providing a precise determination of the power-law exponent in the neutron flux, namely $p=0.956 \pm 0.001$. The neutron flux was then fit to the known ^{103}Rh data, resulting in a final error of 5% in the neutron flux. This uncertainty is the dominant error in the measured neutron widths, since the statistical error is about 0.1%.

The capture widths could not be determined for all measured resonances. Often there were resonances from other nuclei close to the energy of a ^{103}Rh resonance, and these overlapping resonances made it difficult to determine the resonance line shape. For a number of the weaker p-wave resonances, the small number of counts in the peak over a

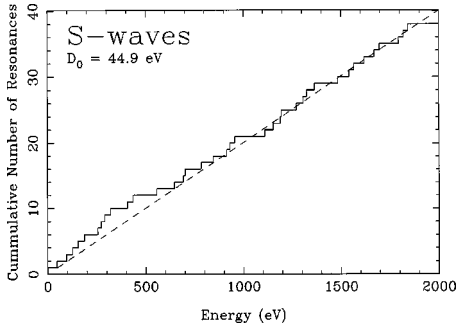

FIG. 3. Cumulative number of s-wave resonances. The line is a linear fit to all data. The value $D_0=44.9$ eV is the s-wave level spacing corrected for missing levels.

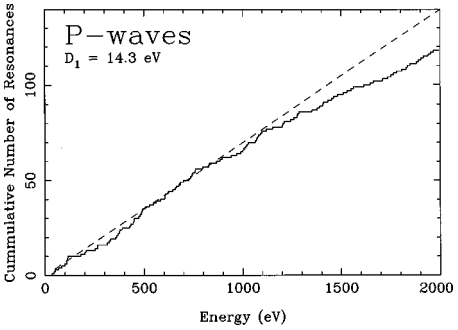

FIG. 4. Cumulative number of p-wave resonances. The line is a linear fit to data below 850 eV. The value $D_1 = 14.3$ eV is the observed p-wave level spacing.

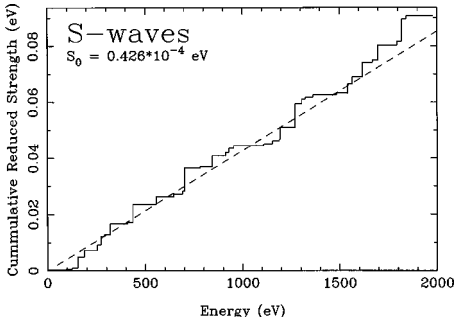

FIG. 5. Cumulative neutron reduced widths for ^{103}Rh s-wave resonances. The line is a linear fit to data below 1200 eV.

limited number of data bins made it difficult to determine the radiative widths for these states. Determination of the Γ_γ value depends critically on knowledge of the resonance spin. The spins of many of the s-wave resonances were determined in earlier γ-ray cascade experiments [21]. In these previous measurements the spins were determined for 25 s-wave resonances up to 1.2-keV neutron energy. In the present work no individual γ-ray spectra were measured, but the spins of a number of s-wave resonances were determined from the relationship between the neutron width and the total capture width [22].

In neutron capture measurements the area of the peak is determined by both $g\Gamma_n$ and the radiative width Γ_γ. When $g\Gamma_n$ is small compared to Γ_γ, the peak area is mainly sensitive to $g\Gamma_n$, so that an average value of Γ_γ may be used in fitting the resonance. If $g\Gamma_n$ is stronger there are problems determining its value from a single capture experiment. When $g\Gamma_n$ is within a factor of two of Γ_γ, then the neutron width cannot be determined from the present data. Qualitatively this is clear from the expression for the limiting case of a thin sample

$$\frac{1}{A_\gamma} = \frac{1}{(g\Gamma_n)} + \frac{1}{g\Gamma_\gamma}. \tag{1}$$

Here A_γ is the properly normalized capture area and g is the statistical factor

$$g = \frac{(2J+1)}{(2i+1)(2I+1)}, \tag{2}$$

where J is the total angular momentum of the s-wave resonance, I is the spin of the target nucleus, and i is the spin of the captured neutron. For ^{103}Rh, J can be either 0 or 1, $I = 1/2$, and $i = 1/2$, which results in $g = 1/4$ for $J = 0$, and $g = 3/4$ for $J = 1$. The radiative width for the different neutron resonances should be approximately constant. Since there is a large difference between g for the different J values, different assumptions for the resonance spin result in large differences in the determination of the radiative width. If $g\Gamma_n$ is close to the value of the average radiative width, an incorrect assumption for J can result in an unphysical value of the radiative width. For the 1619-, 1696-, 1819-, and 1980-eV resonances the J value could be determined with this method. This method was also used in earlier experiments, where the J values of the 929.5-, 1272-, 1306-, 1364-, 1567-, and 1795-eV resonances were inferred in this manner [16]. Both sets of results are listed in Table I, and whether the resonance spins were determined in the present work or in earlier measurements is noted.

The background in the data was determined in each fitting range, where a fitting range included one to eight resonances. The background was assumed to have a quadratic energy dependence, and was fit to the data in a given range and subtracted.

The results of the neutron parameters obtained from our analysis are listed in Table I. The major limitation in the resonance analysis arose at higher energies due to resolution limits. Above about 1500 eV there are often an insufficient number of data points for a detailed analysis—the resonances are spread over too few channels. For completeness we have included in Table I resonance parameters from earlier measurements when appropriate [16,17,21]. In the present experiment six new resonances were identified in ^{103}Rh; these are indicated in Table I. These new identifications were all for p-wave resonances that were not observed before because of lower neutron flux. Although the uncertainty in the neutron flux limits the accuracy of our resonance analysis, the greatly increased neutron flux in the present experiment relative to earlier experiments is a major advantage. In practice we were able to increase the accuracy of the s- and p-wave neutron widths in the region above 150 eV. This high statistics measurement also enabled the determination of new radiative widths for 12 resonances, of which five were p-wave resonances and seven were s-wave resonances. From these an average radiative width for s-wave and p-wave resonances was found, and these are listed in Table II. These values are consistent with the systematics of radiative widths. [17]

IV. ORBITAL ANGULAR MOMENTUM

After the neutron resonance parameters were determined from the data, the probability that a resonance was s-wave or p-wave was estimated. The estimate that a given resonance has an orbital angular momentum of one was calculated with a Bayesian analysis. This analysis, developed by Bollinger and Thomas [23], assumes that the neutron reduced widths obey the Porter-Thomas distribution. Because of the large

TABLE I. Neutron resonance parameters for ^{103}Rh. Some parameters from previous experiments are included (from Ref. [17]) for completeness. The angular momentum l was determined by a Bayesian analysis (see text), and the calculated probability that the resonance has $l=1$ is listed in the column labeled B.P.

Energy (eV)	J	l	B.P.	$g\Gamma_n$ (meV)	Γ_γ (meV)	$g\Gamma_n^l$ (meV)	
1.257±0.002	1	0	0.00	0.39±0.01	155± 5	0.343±0.009	a
34.46±0.02		1	0.97	0.0118±0.0006	154± 3	30.3±1.5	
44.47±0.02		1	0.98	0.0028±0.0001		4.9±0.2	
46.84±0.02	1	0	0.22	0.39±0.02	169± 4	0.057±0.003	
51.92±0.03		1	0.98	0.00088±0.00004		1.21±0.06	
68.33±0.03	1	1	0.92	0.154±0.008	183±16	141.0±7.1	
83.51±0.04		1	0.97	0.0076±0.0004	130±11	5.2±0.3	
95.71±0.05	1	0	0.03	1.60±0.08	179±13	0.16±0.01	
98.77±0.05		1	0.96	0.059±0.003	178±19.58	31.1±1.6	b
108.78±0.06		1	0.96	0.0092±0.0005	100±80	4.2±0.2	b
110.80±0.06		1	0.95	0.126±0.006	152±16	55.8±2.8	
112.62±0.06[e]		1	0.96	0.0083±0.0004		3.6±0.2	
113.99±0.06		1	0.95	0.087±0.004	190±17	37.1±1.9	
125.57±0.07	1	0	0.00	4.7±0.2	182±20	0.42±0.02	
154.57±0.09	0	0	0.00	50±5	170±20	4.0±0.4	c
179.32±0.10		1	0.95	0.125±0.006	174±20	26.9±1.3	b
187.18±0.11	1	0	0.00	31.2±1.6	148±17	2.3±0.1	
199.69±0.11		1	0.95	0.042±0.002		7.7±0.4	
205.01±0.12		1	0.95	0.076±0.004	180±60	13.4±0.7	b
251.13±0.15		1	0.94	0.077±0.004		10.0±0.5	
253.94±0.15	1	0	0.00	31.0±1.5	167±30	1.9±0.1	b
263.12±0.16		1	0.88	0.91±0.05	218±50	110.9±5.5	b
264.21±0.16		1	0.92	0.39±0.02		46.5±2.3	
272.32±0.17	1	0	0.00	51.0±2.5	160±20	3.1±0.2	b
289.90±0.18	1	0	0.00	10.1±0.5	154±40	0.59±0.03	b
312.46±0.20		1	0.94	0.114±0.006		10.7±0.5	
319.77±0.20	1	0	0.00	67.5±7.5	160±17	3.8±0.4	c
321.63±0.20		1	0.90	0.77±0.04		69.1±3.5	
327.75±0.21		1	0.93	0.35±0.02	183±60	30.1±1.5	b
353.89±0.23		1	0.94	0.070±0.003		5.4±0.3	
362.49±0.23		1	0.93	0.28±0.01		21.1±1.1	
366.30±0.24		1	0.86	1.48±0.07	132±25	109.1±5.5	b
373.93±0.24		1	0.92	0.42±0.02	164±80	30.4±1.5	b
376.31±0.25		1	0.93	0.113±0.006		8.0±0.4	
388.62±0.26		1	0.93	0.212±0.011		14.3±0.7	
406.24±0.27	1	0	0.12	9.5±0.5	182±30	0.47±0.02	b
427.59±0.29		1	0.93	0.086±0.004		5.0±0.3	
432.91±0.29		1	0.90	0.88±0.04		50.6±2.5	
435.71±0.30	1	0	0.00	133±20	147±15	6.3±1.0	d
443.93±0.30		1	0.93	0.202±0.010		11.2±0.6	
447.06±0.30		1	0.93	0.136±0.007		7.4±0.4	
449.99±0.31	1	1	0.79	3.01±0.15	147±50	163.3±8.2	b
472.83±0.33		1	0.90	0.92±0.05		46.3±2.5	
479.15±0.33[e]		1	0.93	0.051±0.003		2.5±0.1	
486.44±0.34		1	0.90	0.96±0.06		46.4±2.7	
489.23±0.34		1	0.92	0.135±0.008		6.5±0.4	
492.01±0.34		1	0.85	2.3±0.1	161±50	107.1±6.4	b
504.70±0.36		1	0.92	0.46±0.03		20.8±1.3	
526.01±0.37		1	0.91	0.60±0.04		25.9±1.8	
546.97±0.39		1	0.92	0.065±0.005		2.6±0.2	
555.53±0.40	1	0	0.00	65±15	181±20	2.8±0.6	c

TABLE I. *(Continued)*.

Energy (eV)	J	l	B.P.	$g\Gamma_n$ (meV)	Γ_γ (meV)	$g\Gamma_n^l$ (meV)	
560.35±0.41[e]		1	0.92	0.21±0.02		8.1±0.6	
581.76±0.43		1	0.88	1.6±0.1	151±40	60.4±5.0	b
603.30±0.45		1	0.91	0.35±0.03		12.3±1.1	
604.78±0.45		1	0.88	1.77±0.16		61.7±5.4	
607.37±0.45		1	0.92	0.16±0.01		5.4±0.5	
620.71±0.46		1	0.77	4.7±0.4		156.2±14.3	
644.34±0.49		1	0.90	0.89±0.09		28.2±2.7	
646.37±0.49	1	0	0.04	23.4±2.3	164±18	0.92±0.09	b
657.62±0.50[e]		1	0.91	0.14±0.01		4.3±0.4	
663.49±0.51		1	0.77	5.0±0.5	185±45	152.1±15.2	b
676.46±0.52		1	0.88	1.8±0.2	126±70	52.4±5.4	b
683.34±0.53		1	0.87	2.3±0.2	114±65	67.9±7.0	b
692.08±0.54	1	0	0.03	26.6±2.8	164±30	1.0±0.1	b
699.43±0.54		1	0.89	1.3±0.1		36.2±3.9	
702.33±0.55	1	0	0.00	220±20	177±20	8.3±0.8	c
727.12±0.57		1	0.90	0.86±0.10		22.7±2.5	
733.96±0.58[e]		1	0.91	0.074±0.008		1.9±0.2	
741.63±0.59		1	0.88	1.8±0.2		47.0±5.3	
746.79±0.59[e]		1	0.91	0.15±0.02		3.7±0.4	
757.96±0.60		1	0.90	0.71±0.08		17.7±2.1	
759.66±0.61		1	0.87	2.3±0.3		57.2±6.7	
782.60±0.63	1	0	0.46	13.7±1.6	141±28	0.49±0.06	
796.51±0.64		1	0.86	3.0±0.4		68.1±8.3	
827.93±0.68		1	0.91	0.09±0.01		2.0±0.3	
830.66±0.68		1	0.87	2.1±0.3		46.1±5.8	
845.35±0.70	1	0	0.00	115±20	170±20	4.0±0.7	c
867.69±0.72		1	0.90	0.43±0.06		8.8±1.2	
885.22±0.74		1	0.90	0.49±0.07		9.7±1.3	
894.92±0.75		1	0.79	6.2±0.8	129±80	119.9±16.2	b
913.82±0.77	0	0	0.06	34.9±4.8	145±20	1.2±0.2	b
929.45±0.79	[1]	0	0.02	44.7±6.2	152±25	1.5±0.2	b
942.13±0.81	[0]	1	0.90	0.40±0.06	204±50	7.2±1.0	b
955.05±0.82		0	0.20	27.4±3.9		0.9±0.1	
969.11±0.84		1	0.90	0.21±0.03		3.7±0.5	
989.78±0.86		1	0.89	0.7±0.1		11.2±1.6	
1001.32±0.88		1	0.89	0.9±0.1		15.1±2.2	
1007.84±0.88		1	0.90	0.20±0.03		3.2±0.5	
1017.13±0.90		1	0.90	0.17±0.03		2.7±0.4	
1024.06±0.90		1	0.87	2.1±0.3		33.6±5.0	
1027.66±0.91		1	0.88	1.7±0.3		27.1±4.0	
1065.23±0.95		1	0.89	0.21±0.03		3.1±0.5	
1070.99±0.96		1	0.89	0.45±0.07		6.6±1.0	
1076.25±0.97		1	0.79	7.5±1.1	173±80	109.7±16.9	b
1082.01±0.97		1	0.89	0.50±0.08		7.3±1.1	
1092.33±0.99		1	0.89	0.47±0.07		6.7±1.0	
1098.66±0.99		1	0.89	0.60±0.09		8.6±1.3	
1110.2±1.0	1	0	0.60	16.7±2.6	171±40	0.50±0.08	b
1121.5±1.0		1	0.89	0.49±0.08		6.8±1.1	
1151.7±1.1		1	0.88	1.4±0.2		18.2±2.9	
1154.2±1.1	1	0	0.17	37.6±6.0	243±50	1.1±0.2	b
1189.5±1.1		0	0.55	20.5±3.3		0.6±0.1	
1195.9±1.1	0	0	0.00	150.0±82.5	224±60	4.3±2.4	c
1201.6±1.1		1	0.87	2.7±0.4		33.4±5.5	

TABLE I. *(Continued).*

Energy (eV)	J	l	B.P.	$g\Gamma_n$ (meV)	Γ_γ (meV)	$g\Gamma_n^l$ (meV)	
1205.6±1.1		1	0.89	0.53±0.09		6.6±1.1	
1211.4±1.1		1	0.87	2.3±0.4		28.7±4.7	
1244.8±1.2		1	0.86	2.7±0.4		31.6±5.3	
1261.5±4.0		1	0.88	0.9±0.2		9.8±2.0	a
1271.8±1.2	[1]	0	0.00	300±100	185±30	8.4±2.8	c
1276.5±4.0		1	0.87	2.5±2.0		28.4±22.7	a
1279.0±1.2		1	0.85	4.1±0.7		46.5±7.9	
1286.4±1.2		1	0.86	2.8±0.5		32.0±5.4	
1306.0±1.3	[1]	0	0.05	61.7±10.6	154±35	1.7±0.3	b
1324.9±1.3		0	0.52	25.1±4.3		0.7±0.1	
1353.1±1.3		1	0.87	1.7±0.3		17.4±3.0	
1364.5±1.3	[1]	0	0.41	31.7±5.6	184±50	0.9±0.2	b
1379.7±1.4		1	0.86	2.5±0.4		25.8±4.6	
1392.2±1.4		1	0.86	3.1±0.6		31.3±5.6	
1406.9±1.4		1	0.70	16.7±3.0		164.2±29.3	
1410.6±1.4		1	0.87	1.7±0.3		16.8±3.0	
1432.6±1.4		1	0.82	7.1±1.3		67.9±12.2	
1452.3±1.5		1	0.86	2.4±0.4		22.6±4.1	
1462.7±1.5		1	0.88	0.6±0.1		6.0±1.1	
1482.4±1.5		1	0.82	7.4±1.3		66.9±12.2	
1485.8±1.5		0	0.64	22.0±4.0		0.6±0.1	
1510.2±1.5		1	0.87	0.9±0.2		7.8±1.4	
1530.3±1.6		1	0.85	4.4±0.8		37.9±7.0	
1542.8±1.6	0	0	0.00	127.0±7.0	122±61	3.2±0.2	c
1552.0±1.6		1	0.86	3.1±0.6		26.6±5.0	
1561.8±1.6		1	0.79	10.4±2.0		87.8±16.4	
1566.8±1.6	[1]	0	0.02	99.0±6.5	138±41	2.5±0.2	c
1615.9±1.7		1	0.87	1.3±0.3		10.6±2.0	
1619.0±1.7	1[f]	0	0.00	207.0±9.3	152±43	5.1±0.2	b
1647.7±1.7		1	0.87	0.8±0.2		6.1±1.2	
1665.3±1.8		1	0.86	2.6±0.5		19.7±3.8	
1669.9±1.8		0	0.54	32.8±6.3		0.8±0.2	
1696.3±1.8	1[f]	0	0.00	218.5±9.9	171±46	5.3±0.2	d
1709.5±1.8		1	0.86	2.2±0.4		16.3±3.2	
1735.1±1.9		1	0.81	9.1±1.8		65.0±12.7	
1751.5±5.0		1	0.87	1.1±0.4		7.6±3.0	a
1764.4±1.9		1	0.77	14.0±2.8		98.4±19.3	
1780.9±1.9		1	0.86	2.3±0.5		15.9±3.1	
1794.8±2.0	[1]	0	0.24	63.5±5.1	195±70	1.5±0.1	c
1806.0±5.0		1	0.86	1.1±0.5		7.1±3.6	b
1819.6±2.0	1[f]	0	0.00	334.0±16.7	219±52	7.8±0.4	d
1831.2±2.0		1	0.86	1.4±0.3		9.5±2.0	
1836.8±2.0		1	0.84	4.3±0.9		28.3±5.7	
1842.1±2.0	1	0	0.45	45.0±4.5		1.0±0.1	d
1849.2±5.0		1	0.86	2.3±0.7		15.0±4.5	a
1882.0±2.1		1	0.86	1.4±0.3		9.1±1.8	
1890.2±2.1		1	0.86	1.0±0.2		6.6±1.3	
1903.0±2.1		1	0.80	10.4±2.1		65.3±13.2	
1917.5±2.2		1	0.85	2.2±0.5		13.8±2.8	
1940.1±2.2		1	0.84	5.0±1.0		30.6±6.2	
1952.4±2.2		1	0.85	3.7±0.7		22.1±4.5	
1966.2±2.2		1	0.85	2.7±0.6		16.3±3.3	
1980.8±2.3	0[f]	0	0.03	134.0±7.4	158±59	3.0±0. 2	d

TABLE I. *(Continued).*

Energy (eV)	J	l	B.P.	$g\Gamma_n$ (meV)	Γ_γ (meV)	$g\Gamma_n^l$ (meV)
1994.0±2.3		1	0.85	2.4±0.5		14.1±2.9
2008.0±2.3		1	0.73	11.2±2.3		64.4±13.3
2019.4±2.3		1	0.89	1.8±0.4		10.0±2.1

[a]All resonance parameters from Ref. [17].
[b]Γ_γ from Ref. [17].
[c]New resonance energy; $g\Gamma_n$ and Γ_γ from Ref. [17].
[d]$g\Gamma_n$ from Ref. [17].
[e]New resonance identified in this work.
[f]Spin assignment from this work; see discussion in Sec. III.

difference in penetrabilities for s-wave and p-wave resonances, most of the stronger resonances are s wave and the weaker resonances are p wave. The Bayesian probability of a resonance being p wave is [24]

$$\text{B.P.}=\left(1+\frac{4}{9}\sqrt{\frac{4S_1c^0(E)}{3S_0c^1(E)}}\times\exp\left[-\frac{g\Gamma_n c^0(E)}{2D_0}\left(\frac{1}{S_0}-\frac{3c^1(E)}{4S_1c^0(E)}\right)\right]\right)^{-1}, \quad (3)$$

where S_0 and S_1 are the s-wave and p-wave strength functions, D_0 is the average s-wave level spacing, and $g\Gamma_n$ is the neutron width of the state in question. A resonance was assumed to be p wave if the probability B.P. was greater than 69%, and s wave if the probability was less than 69%. To clarify this choice, we remind the reader that the Bayesian conditional probability is defined as

$$\text{B.P.}(l=1|g\Gamma_n)=\frac{P_1{*}P(g\Gamma_n|l=1)}{P_1{*}P(g\Gamma_n|l=1)+P_0{*}P(g\Gamma_n|l=0)}, \quad (4)$$

where P_0 and P_1 are *a priori* probabilities for the resonance to be s or p wave and $P(g\Gamma_n|l=0)$, $P(g\Gamma_n|l=1)$ are the Porter-Thomas probabilities for a given $g\Gamma_n$ value assuming the s- or p-wave nature of the resonance. The B.P. becomes the (B.P.)* if one accepts the choice of equal Porter-Thomas probabilities as a criterium for dividing resonances by parity. With the assumption of the $(2J+1)$ law for level densities, one gets (B.P.)*=67% for all nonzero I nuclei, except those of nuclear spin $I=1/2$, which is the case for ^{103}Rh. For this target there are two spins, $J=0,1$, for s-wave resonances, and this produces a sum of $(2J+1)=4$; and for p-wave resonances there are three total spins, $J=0,1,2$, which produces the sum of $(2J+1)=9$. From the ratio of these sums one gets a (B.P.)*=9/(4+9)=69%. Of course the assignment is less reliable when the probability B.P. is close to the (B.P.)* value.

The functions $c^l(E)$ are

$$c^l(E)=\frac{[1+(kR)^{2l}]}{(kR)^{2l}\sqrt{E(\text{eV})}}, \quad (5)$$

and for the nuclide ^{103}Rh, for $l=0$ and 1,

$$c^0(E)=\frac{1}{\sqrt{E(\text{eV})}} \quad \text{and} \quad c^1(E)=\frac{1}{\sqrt{E(\text{eV})}}\left(\frac{4.6\times10^5}{E(\text{eV})}\right), \quad (6)$$

where the nuclear radius is assumed to be $R=1.35A^{1/3}$ fm. The probabilities depend on the s-wave and p-wave strength functions, and on the average s-wave level spacing. The strength functions were determined in the usual way, by summing the reduced width over a range of energies

$$S_l=\frac{1}{(2l+1)\Delta E}\sum g\Gamma_n^l, \quad (7)$$

and the reduced widths were calculated in the usual way [17],

$$g\Gamma_n^l=c^l(E)g\Gamma_n. \quad (8)$$

The values of the strength functions change as the orbital angular momentum assignments are made. This process of assigning resonances with this probabilistic argument, and then determining the strength functions and level densities was iterated until the values stabilized. The final values for the strength functions and level spacings were insensitive to the change of one or two resonance assignments. The final

TABLE II. Average radiative widths, level spacings, and strength functions for ^{103}Rh.

Values	$\langle\Gamma_{\gamma0}\rangle$ (meV)	$\langle\Gamma_{\gamma1}\rangle$ (meV)	D_0 (eV)	D_1 (eV)	S_0 (10^{-4} eV)	S_1 (10^{-4} eV)
current[a]	164±4	155±6	44.9±3.1	14.3±3.1	0.43±0.08	8.8±1.2
previous[b]	160±15		16±1		0.53±0.05	5.5±0.9

[a]Values from this work. Uncertainties of $\langle\Gamma_{\gamma0}\rangle$ and $\langle\Gamma_{\gamma1}\rangle$ are calculated from variances of the corresponding Γ_γ distributions.
[b]Values from Mughabghab *et al.* [17].

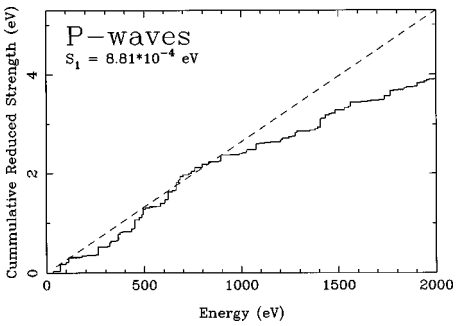

FIG. 6. Cumulative neutron reduced widths for ^{103}Rh p-wave resonances. The line is a linear fit to data below 850 eV.

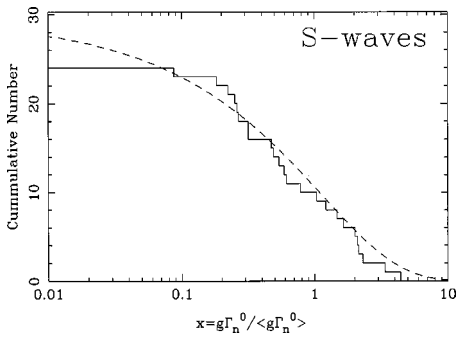

FIG. 7. Cumulative neutron reduced width distributions for s-wave resonances compared to the Porter-Thomas distribution.

probabilities are listed in Table I under the column labeled B.P., along with the neutron resonance parameters.

From these assignments, plots of the cumulative number of states as a function of energy were made and compared to the values for the average level spacings. These are shown in Figs. 3 and 4. Plots of the cumulative reduced strength for s-wave and p-wave resonances are shown in Figs. 5 and 6. Above a certain energy resonances are missed because of the decreasing experimental resolution. In plots of the cumulative number of states or the cumulative reduced strength, this is indicated by the experimental curve falling below the linear extrapolation, where the lines are linear fits to the data in the low energy regions. The average level spacings are determined from the range of energies over which the cumulative number of levels is linear. The determination of the strength functions was also limited to these energy ranges. Over limited energy ranges the measured curves agree with the linear extrapolations, but for both s- and p-wave resonances the measured curves fall away above these limited energy ranges. Of course, while a strong deviation from linearity is a clear sign that levels are being missed, the opposite is not true. If a constant fraction of the levels is missed, then the plots are still linear. Thus one uses data in the linear range as a starting point for more detailed analysis. For s-wave resonances this energy cutoff is about 1200 eV, and for p-wave resonances the energy cutoff is about 850 eV. The choice of 850 eV for p waves is clear from consideration of Figs. 4 and 6. For s-wave levels we choose 1200 eV to reduce uncertainties in results due to the statistical unreliability of the Bayesian procedure when $P \simeq (\text{B.P.})^*$. The strength functions and level spacings determined from these energy regions are listed in Table II. The strength function values are consistent with those values determined from previous measurements [16,17], while the spacing value is not. We assume that the value listed in the compilation is a typographical error, since the value quoted there is inconsistent with the actual table of resonance parameters listed by Mughabghab *et al.* [17].

V. STATISTICAL TESTS

The distribution of the neutron reduced widths is expected to agree with the Porter-Thomas distribution [17,25]

$$P(y) = \frac{e^{-y/2}}{\sqrt{2\pi y}}, \quad \text{where} \quad y = \frac{g\Gamma_n^l}{\langle g\Gamma_n^l \rangle}. \tag{9}$$

In Figs. 7 and 8, the cumulative numbers of resonances are compared with the integral of the Porter-Thomas distribution. Since states of smaller size are more likely to be missed, the integral of the distribution is shown from larger to smaller values. We note that the total number of levels under the full theoretical distribution is 8% larger than the number of levels in the theoretical distribution above the $y = 10^{-2}$ cutoff shown in the figures. The theoretical curves on Figs. 7 and 8 were normalized by making fits to the experimental histograms in the region of $0.2 < x < 5.0$—the region which is least prone to the missing levels. Comparison with the histograms indicates that about 10% of the s-wave resonances have been missed below 1.2 keV, and that about 22% of the p-wave resonances have been missed below 850 eV.

For a sequence of compound nuclear states with the same symmetry, the level statistics are expected to obey predictions of the Gaussian orthogonal ensemble version of random matrix theory [26,27]. To a good approximation, the nearest neighbor spacing distribution should obey the Wigner distribution

$$P(x) = \frac{\pi}{2} x e^{-(\pi x^2/4)}, \quad \text{where} \quad x = \frac{D_{li}}{\langle D_l \rangle}. \tag{10}$$

The other extreme, corresponding to no level repulsion or long range correlations, is the Poisson distribution e^{-x}. In our experiment there are two spins for the s-wave resonances

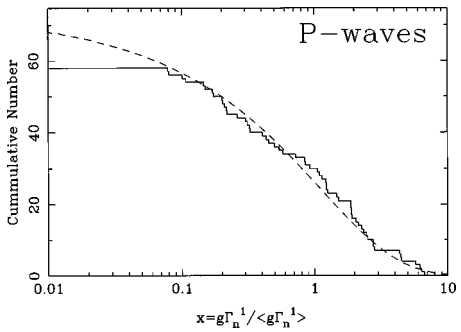

FIG. 8. Cumulative neutron reduced width distributions for p-wave resonances compared to the Porter-Thomas distribution.

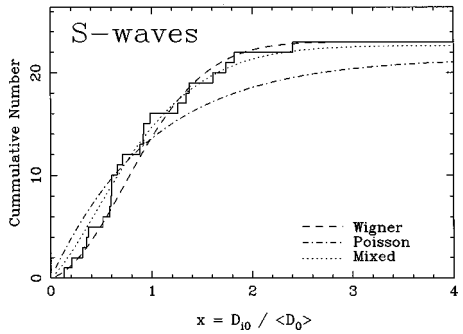

FIG. 9. Nearest neighbor spacing distribution for the *s*-wave resonances up to 1000 eV. The experimental distribution is compared with the Wigner distribution, the mixed two-sequence distribution (see text), and the Poisson distribution.

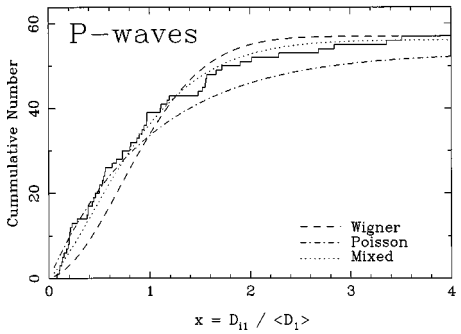

FIG. 10. Nearest neighbor spacing distribution for the *p*-wave resonances up to 1000 eV. The experimental distribution is compared with the Wigner distribution, the mixed three-sequence distribution (see text), and the Poisson distribution.

and three spins for the *p*-wave resonances. Therefore we should observe a linear combination of two *s*-wave GOE sequences and three *p*-wave GOE sequences. The relative weight is determined by the relative level densities. For this target nucleus—with spin 1/2—the appropriate relative densities are 1/4 and 3/4 for the *s*-wave resonances, and 1/9, 3/9, and 5/9 for the *p*-wave resonances. The numerical results are plotted in Figs. 9 and 10 for the Wigner distribution, the Poisson distribution, and the mixed Wigner distribution, and compared to the data. The distributions are normalized to the data such that they agree at infinity. Considering the fraction of levels missed the agreement with the GOE prediction is reasonable.

VI. SUMMARY

We have measured neutron resonances in ^{103}Rh from 30 eV to 2 keV using radiative capture. A total of six new resonances were identified in this work. We also have increased the accuracy in the determination of the resonance energies and most of the neutron widths, as well as the radiative widths for 15 resonances. The orbital angular momentum assignment was performed with a Bayesian analysis. In the present experiment 90% of the *s*-wave resonances below 1.2 keV, and 78% of the *p*-wave resonances below 850 eV, were observed. In this energy range new values were calculated for the average level spacing and strength function for both *s*-wave and *p*-wave resonances. These results are consistent with previous measurements. These resonance parameters were then used in the analysis of parity violation data on ^{103}Rh [28] which will be described in the following paper.

ACKNOWLEDGMENTS

W. M. Snow, C. Keith, and D. Rich provided data on neutron flux measurements with ^{3}He, which were crucial for our analysis of the present data. The authors would also like to acknowledge W. S. Wilburn for valuable discussions during the preparation of this paper. This work was supported in part by the U.S. Department of Energy, Office of High Energy and Nuclear Physics, under Grant Nos. DE-FG02-97-ER41042 and DE-FG02-97-ER41033, and by the U.S. Department of Energy, Office of Energy Research, under Contract No. W-7405-ENG-36.

[1] V. P. Alfimenkov, S. B. Borzakov, Vo Van Thuan, Yu. D. Mareev, L. B. Pikelner, A. S. Khrykin, and E. I. Sharapov, Nucl. Phys. **A398**, 93 (1983).
[2] J. D. Bowman, G. T. Garvey, Mikkel B. Johnson, and G. E. Mitchell, Annu. Rev. Nucl. Part. Sci. **43**, 829 (1993).
[3] V. V. Flambaum and G. F. Gribakin, Prog. Part. Nucl. Phys. **35**, 423 (1995).
[4] G. E. Mitchell, J. D. Bowman, and H. A. Weidenmüller, Rev. Mod. Phys. **71**, 435 (1999).
[5] J. D. Bowman *et al.*, Phys. Rev. Lett. **65**, 1192 (1990).
[6] C. M. Frankle *et al.*, Phys. Rev. Lett. **67**, 564 (1991).
[7] B. E. Crawford *et al.*, Phys. Rev. C **58**, 1225 (1998).
[8] S. L. Stephenson *et al.*, Phys. Rev. C **58**, 1236 (1998).
[9] J. D. Bowman, L. Y. Lowie, G. E. Mitchell, E. I. Sharapov, and Yi-Fen Yen, Phys. Rev. C **53**, 285 (1996).
[10] D. A. Smith *et al.*, Bull. Am. Phys. Soc. **42**, 1071 (1997).
[11] P. W. Lisowski, C. D. Bowman, G. J. Russell, and S. A. Wender, Nucl. Sci. Eng. **106**, 208 (1990).
[12] C. M. Frankle, J. D. Bowman, S. J. Seestrom, N. R. Roberson, and E. I. Sharapov, *Time Reversal Invariance and Parity Violation in Neutron Resonances*, edited by C. R. Gould, J. D. Bowman, and Yu. P. Popov (World Scientific, Singapore, 1994) p. 204.
[13] B. E. Crawford *et al.*, in *IV International Seminar on Interactions of Neutrons with Nuclei*, JINR Report No. E3-96-336 (Joint Institute of Nuclear Research, Dubna, 1996), p. 268.
[14] S. J. Seestrom *et al.*, Nucl. Instrum. Methods Phys. Res. A (to be published).
[15] J. D. Bowman, Y. Matsuda, Y.-F. Yen, and B. E. Crawford (unpublished).
[16] P. Ribon, J. Gigard, and J. Trochon, Nucl. Phys. **A143**, 130 (1970).
[17] S. F. Mughabghab, M. Divadeenam, and N. E. Holden, *Neutron Cross Sections*, Vol. 1, Part A (Academic Press, New York, 1981).

[18] S. L. Stephenson *et al.*, in *IV International Seminar on Interactions of Neutrons with Nuclei* [13], p. 171.
[19] G. J. Russell, J. S. Gilmore, H. Robinson, G. L. Legate, A. Bridge, R. J. Sanchez, R. J. Brewton, R. Woods, and H. G. Hughes III, in *Proceedings of the 10th International Collaboration of Advanced Neutron Sources*, edited by Diana Higher, AIP Conf. Proc. No. 97 (AIP, New York, 1989), p. 483.
[20] D. Rich *et al.*, submitted to Phys. Rev. A.
[21] T. J. Haste and B. W. Thomas, J. Phys. G **1**, 981 (1975).
[22] L. Y. Lowie *et al.*, Phys. Rev. C **56**, 90 (1997).
[23] L. M. Bollinger and G. E. Thomas, Phys. Rev. **171**, 1293 (1968).
[24] C. M. Frankle, E. I. Sharapov, J. A. Harvey, N. W. Hill, and L. W. Weston, Phys. Rev. C **50**, 2774 (1994).
[25] C. E. Porter and G. E. Thomas, Phys. Rev. **104**, 483 (1956).
[26] T. A. Brody, J. Flores, J. B. French, P. A. Mello, A. Pandey, and S. S. M. Wong, Rev. Mod. Phys. **53**, 385 (1981).
[27] T. A. Guhr, A. Müller-Groeling, and H. A. Weidenmüller, Phys. Rep. **299**, 189 (1998).
[28] D. S. Smith *et al.*, Phys. Rev. C **60**, 045503 (1999), following paper.